

Multi-physics analysis for the design and development of micro-thermoelectric coolers

Seung Woo Han*, MD Anwarul Hasan*, Jung Yup Kim*, Hyun Woo Lee**, Kong Hoon Lee***, and Ook Joong Kim***

* Micro System and Structural Mechanics Group, Korea Institute of Machinery & Materials, Daejeon, Korea
(Tel : +82-42-868-7884; E-mail: swhan@kimm.re.kr, anwer@kimm.re.kr, jykim@kimm.re.kr)

**Department of Mechanical Engineering, Pusan National University, Pusan, Korea
(Tel : +82-0-000-0000; E-mail: hywlee@hyowon.pusan.ac.kr)

***HVAC and Cryogenic Engineering Group, Korea Institute of Machinery & Materials, Daejeon, Korea
(Tel : +82-42-868-7884; E-mail: konghoon@kimm.re.kr, ojkim@kimm.re.kr)

Abstract: A rigorous research is underway in our team, for the design and development of high figure of merits ($ZT = 1.5 \sim 2.0$) micro-thermoelectric coolers. This paper discusses the fabrication process that we are using for developing the Sb_2Te_3 - Bi_2Te_3 micro-thermoelectric cooling modules. It describes how to obtain the mechanical properties of the thin film TEC elements and reports the results of an equation-based multiphysics modeling of the micro-TEC modules. In this study the thermoelectric thin films were deposited on Si substrates using co-sputtering method. The physical mechanical properties of the prepared films were measured by nanoindentation testing method while the thermal and electrical properties required for modeling were obtained from existing literature. A finite element model was developed using an equation-based multiphysics modeling by the commercial finite element code FEMLAB. The model was solved for different operating conditions. The temperature and the stress distributions in the P and N elements of the TEC as well as in the metal connector were obtained. The temperature distributions of the system obtained from simulation results showed good agreement with the analytical results existing in literature. In addition, it was found that the maximum stress in the system occurs at the bonding part of the TEC i.e. between the metal connectors and TE elements of the module.

Keywords: Multi-Physics Analysis, Thermoelectric coolers, Phonon, Nanoindentation test, Von misses stress

1. INTRODUCTION

TEC (Thermo Electric cooler) modules show excellent cooling performance for the applications where temperature stabilization, temperature cycling or cooling below ambient is required. Due to their excellent performance, TEC are widely used in numerous products, including CCD (charge coupled device) cameras, laser diodes, infrared detectors, microprocessors, blood analyzers, portable picnic coolers as well as many other applications in aerospace [1], bioengineering [2, 3] and semiconductor industries. Recent suggestion by Dresselhouse et al. [4] that nanoengineering of thermoelectric (TE) materials could result in higher values of ZT (thermoelectric figure of merit), and the findings of Venkatasubramanian et al. [5] that a ZT value of 2.4 can be achieved in Sb_2Te_3 / Bi_2Te_3 thin films near 1 nm thickness, have given enormous momentum to the research on micro-TEC. Although TEC modules in the range of millimeter and centimeter sizes are widely commercially available these days, the micro-TEC devices are still in the research and development stage. Some of the recent works on fabrication of thin film for micro-TEC include those of H. Zou et al. [6, 7], Min and Rowe et al. [8], J.P. Fleurial et al. [9] and so on. Numerical study on micro-TEC has also gained attention of researchers. One of the example of which is the study of Alexandru et al. [1], where they have performed FEM analysis of thermoelectric phenomena in semiconductor materials.

In this paper, we have developed an equation-based multiphysics model using the FEM code FEMLAB, for exploring the physical insights of micro-TEC. The fabrication process of the micro-TEC has been discussed. Various properties required for FE modeling have been obtained and thermal and structural analysis of the TEC have been performed. The model developed in this study will be helpful in reducing the time and cost of the design and development of micro-TEC significantly in our ongoing research.

2. WORKING PRINCIPLE OF A TEC

Fig. 1 shows the schematic picture of a typical TEC. In general a TEC consists of a series of P type and N type thermoelectric (doped semiconductor) materials sandwiched between two ceramic wafers. The TE materials are connected electrically in series and thermally in parallel through metal connectors on both sides. When a DC current passes through these materials, three different effects take place simultaneously, namely: the Peltier effect, Joule heating effect and heat transfer by conduction due to the temperature difference between the hot and the cold junctions.

It is generally known that electrons in P-type materials have lower energy state and those in N-type materials have higher energy state. As the electrons move from the P type to the N type material through an electrical connector the electrons jump to a higher energy state absorbing thermal energy from the cold side plate, but when these high energy electrons move from N type to P type material through the metal connector attached to the hot plate, they release their extra thermal energy. Thus the electrons, as they pass through the P and N

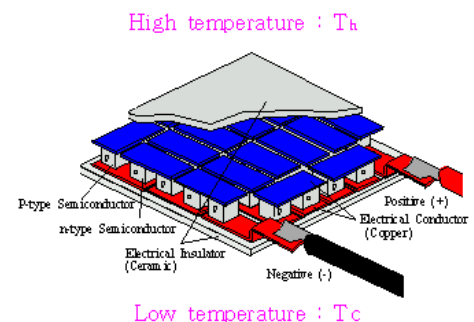


Fig. 1 Schematic picture of a TEC module.

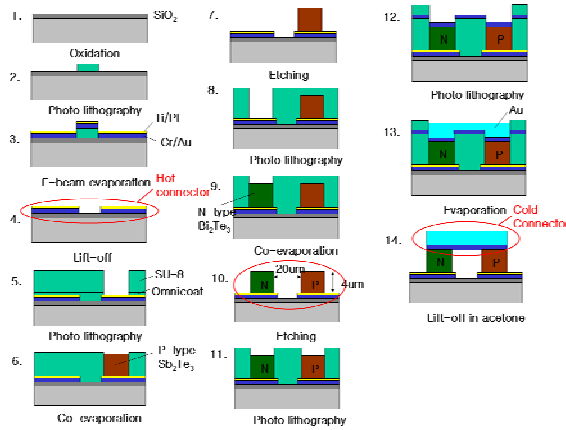


Fig. 2 Fabrication process of micro thermoelectric cooling module.

type materials alternatively, carry heat from the cold to the hot plate and provide cooling effect.

3. FABRICATION PROCESS OF MICRO TEC

The fabrication procedure that we are to use for making the micro-TEC is shown in Fig. 2. The processing route is based on the thin film technology and MEMS processes. There are numerous methods available for thin film deposition of the TE films, including flash evaporation [10], hot wall epitaxy [11], pulsed laser deposition [12], metal organic chemical vapour deposition [13] and molecular beam epitaxy [14]. We, in our research, are using the co-sputtering method (instead of co-evaporation in step 6 and 9 of Fig. 2) using an RF magnetron sputtering equipment. The SiO₂ layer developed on the Si wafer as shown in step 1 of Fig. 2 serves as the electric insulator. For deposition of the metal connector layer in step 3 and step 13 physical vapor deposition (evaporation) method is used. Details of other steps in Fig. 2 such as photo-lithography, lift off and etching can be found elsewhere in literature [15].

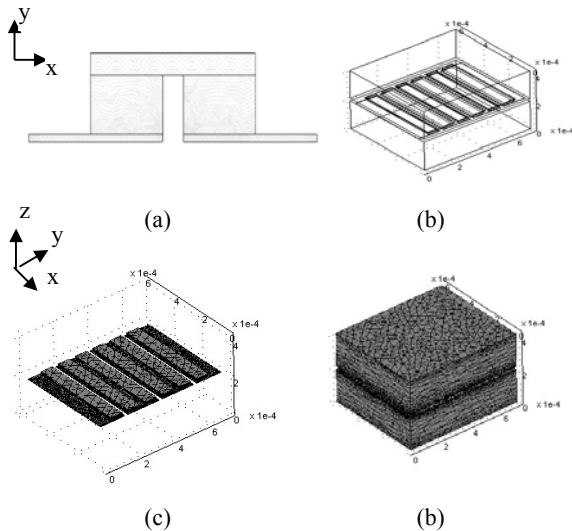


Fig. 3 Model geometry: (a) 2D mesh model, (b) 3D geometry, (c) mesh showing TE elements and (d) 3D complete mesh model.

4. MULTIPHYSICS MODELING

4.1 Model geometry

A simplified 2D model which consisted of a single pair P and N column of thermoelectric alloys along with metal (Cu) connectors on top and bottom of the TE columns as shown in Fig. 3(a) was developed for validation of the multiphysics modeling approach used in this study. The approach was then extended to three dimensions. The 3D model developed in this study consisted of three pairs of TE couples connected electrically in series through top and bottom metal connectors and thermally in parallel as shown in Figs. 3(b) and (c). The thermoelectric couples along with the metal connectors were sandwiched between two silicon substrates, which served as the hot and cold plate of the TE cooler. The dimensions of the substrates, connectors and TE elements were 700x600x200 μm, 140x515x2 μm and 65x500x10 μm respectively.

4.2 Governing equations

The transport of electrons in a thermoelectric material can be modeled using Boltzmann transport equation (BTE). However, the boundary resistances in the metal-thermoelectric boundary interfaces hinder the phonon heat flow differently than the electronic heat flow and cause electron-phonon thermal non-equilibrium near the interfaces. Moreover the mutual interaction of electron and phonon affects the thermal and electrical transport processes and hence the temperature distributions of both the electrons and phonons in the TE material. Therefore, to obtain the electron and phonon temperature distribution in TE materials of a TEC we need the coupled Boltzmann transport equation given by

$$-\nabla \cdot (k_p \nabla T_p) = P(T_e - T_p) \quad (1)$$

$$-\nabla \cdot (k_e \nabla T_e) = \rho_e j_e^2 - P(T_e - T_p) \quad (2)$$

$$\text{where } P = \frac{n_e k_B}{\tau_e}$$

Descriptions of the symbols used in above equations and of those that will come forward are provided in the nomenclature section at the end of the paper. For simplification, as well as for proving the validation of our approach we used a one-dimensional approach as followed by Da Silva and Kaviany [16]. The coupled BTE then reduced to the form

$$-k_e \frac{d^2 T_e}{dx^2} = \rho_e j_e^2 - P(T_e - T_p) \quad (3)$$

$$-k_p \frac{d^2 T_p}{dx^2} = P(T_e - T_p) \quad (4)$$

The boundary conditions for the model are

$$\left. \frac{T_h - T_p}{(A_e R_c)_{b,p}} \right|_{-L_w/2} = -k_p \frac{dT}{dz} \Big|_{-L_w/2} \quad (5)$$

$$\left. \frac{T_p - T_c}{(A_e R_c)_{b,pp}} \right|_{+L_w/2} = -k_p \frac{dT}{dz} \Big|_{+L_w/2} \quad (6)$$

$$\left. \frac{T_h - T_e}{(A_e R_c)_{b,ee}} \right|_{-L_w/2} = -k_e \frac{dT_e}{dz} \Big|_{-L_w/2} + \Delta \alpha \cdot j_e T_e \Big|_{-L_w/2} - (A_e R_e)_b \frac{j_e^2}{2} \quad (7)$$

$$\left. \frac{T_e - T_c}{(A_{te} R_c)_{b,ee}} \right|_{+L_w/2} = -k \left. \frac{dT_e}{dz} \right|_{+L_w/2} + \Delta \alpha \cdot j_e T_e \Big|_{+L_w/2} + (A_{te} R_e)_b \frac{j_e^2}{2} \quad (8)$$

The non-linear coupled set of equations (3) and (4) was modeled in the FEMLAB by selecting the general form of the PDE (Partial Differential Equation) given by

$$\nabla \cdot (-c \cdot \nabla u - \alpha u + \gamma) + \beta \cdot \nabla u + \alpha u = f \quad (9)$$

The α , β and γ in Eqn. 9 represents the conservative flux convection coefficient, the convection coefficient and the conservative flux term respectively. Considering $\alpha = 0$, $\beta = 0$ and $\gamma = 0$, the Eqn. 9 becomes

$$-c \cdot \nabla^2 u + \alpha u = f \quad (10)$$

A comparison between Eqn. 3 and Eqn. 10 yields $T_e = u$, $k_e = c$, $a = P$ and $f = \rho_e j_e^2 + P T_p$. Similarly, by comparing Eqn. 4 with Eqn. 10 we obtain $T_p = u$, $k_p = c$, $a = P$ and $f = P T_e$. Thus the governing equations (Eqn. 3 and Eqn. 4) were implemented in the FEMLAB through Eqn. 10 by using the constants as mentioned.

4.3 Electrical and thermal properties

The electrical and thermal properties of the Bi_2Te_3 and Sb_2Te_3 used in the model, obtained from ref. [16] are shown in Table 1. The boundary thermal and electrical resistances for the electron and phonon [16] are presented in Table 2.

4.4 Mechanical properties

For structural analysis of the model the mechanical properties are required. The Young's modulus and the Poisson's ratios were obtained using the nanoindentation method. Hardness of the materials were also measured from nanoindentation test results. The tests were performed using a nanoindentation XP with the Berkovich tip indenter, as shown in Fig. 4. Maximum indentation depth was 1000 nm. Fig. 5 shows a typical modulus versus displacement curve and hardness versus displacement curve as well as the nanoindentation mark on a Bi_2Te_3 sample. Results obtained from the nanoindentation test are shown in Table 3.

Table 1. Electrical and thermal properties of the TE materials used in the model.

Property	Symbol	Bi_2Te_3	Sb_2Te_3
Seeback coefficient	α ($\mu\text{V/K}$)	-228	171
Electron thermal conductivity	k_e (W/mK)	0.5	0.6
Phonon thermal conductivity	k_p (W/mK)	1.5	1.5
Electrical resistivity	ρ (Ωm)	1.30×10^{-5}	1.04×10^{-5}
Cooling length	δ (nm)	66	156

Table 2. Boundary Resistances used in the model.

Property	Bi_2Te_3	Sb_2Te_3
Phonon boundary resistance	9.2×10^{-8}	8.0×10^{-8}
Electron boundary resistance	3.5×10^{-7}	9.3×10^{-7}
Electrical boundary resistance	2.6×10^{-12}	6.8×10^{-12}

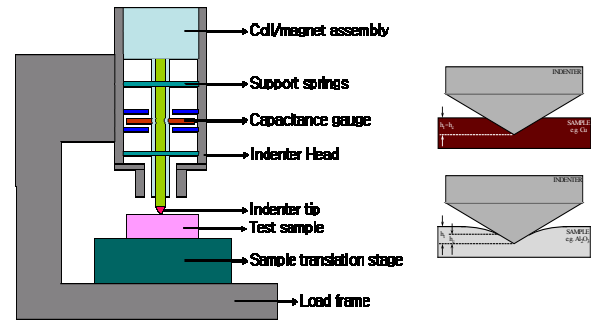


Fig. 4 Schematic diagram of a nanoindentation tester.

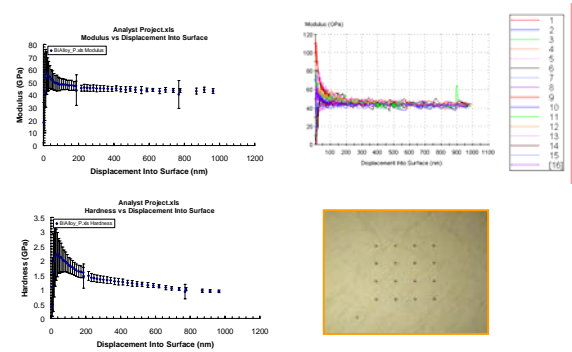


Fig. 5 Result of nanoindentation test on Bi_2Te_3 Sample.

Table 3. Results of Nanoindentation.

Sample	Modulus(GPa)	Hardness(GPa)
Sb_2Te_3 (Bulk)	44.823	1.23
Bi_2Te_3 (Bulk)	41.799	1.259
Bi_2Te_3 (film)	48.325	2.750
Cu	229.706	6.654

4.5 Solving the model

The developed 2D model was solved numerically for the operating conditions, $T_h = 285$ K, $T_c = 300$ K and $J_e = 0, 15$ and 30 mA. The 3D model when solved for the same operating conditions did not show any significant change in temperature and stress distributions, which indicate that $0, 15$ and 30 mA currents are not sufficient to cause thermoelectric heat flow in the TEC module. The 3D model was then solved for the same hot side and cold side temperature but higher current inputs i.e. for $T_h = 300$ K, $T_c = 285$ K and $J_e = 4, 8, 12, 16$ and 20 A. To reduce the computation time Lagrangian linear elements were selected.

5. RESULTS AND DISCUSSION

The phonon and electron temperature distributions in the

2D simplified model for $T_c = 285$ K, $T_h = 300$ K and $J_e = 30$ mA are shown in Figs. 6(a) and (b), while the total displacement and stress developed in the model are shown in Figs. 6(c) and (d) respectively. Figs. 7 and 8 represent the variations of electron and phonon temperatures along the height of the Bi_2Te_3 (N type) and Sb_2Te_3 (P type) TE columns for different current (0, 15 and 30 mA) inputs.

It can be noticed that for $J_e = 0$ i.e. for no thermoelectric effect, the electron and phonon temperatures (T_e and T_p) are same. But as J_e increases, the difference between T_e and T_p near the junction increases.

The deviations of T_e and T_p at the hot junctions are higher than those at the cold junction. The reason is quite clear: at the cold junction (i.e. at $x = -2$ μm) the values of T_e and T_p decreases with peltier cooling and increases with Joule heating, but at the hot junction (i.e. at $x = 2$ μm) both the peltier effect and Joule heating effect raises the values of T_e and T_p . Thus the deviations at hot junction are always higher than those at the cold junction. All these trends of the curves as well as their pattern and values are similar to those obtained by L.W. da Silva et al. through analytical solutions for same operating conditions. These consistencies prove the validation of our model and approach of study.

The Von misses equivalent stress developed in the model is shown in Fig. 6(d), while the variation of Von misses stress along the length of P and N type TE columns are shown in Fig. 9. It is evident from Fig. 9 that the maximum stress in the model occurs at the interface between the hot connector and the P type TE column. The curves for both the N type and P type columns show that the most vulnerable location for failure due to thermal stress are the end points of the column-metal connector interfaces. While the maximum stress developed at the N-type column-metal connector interface was 80 Mpa, the maximum stress for the P-type column was 125 Mpa. The higher stresses in the N-type thermoelectric column are due to the higher temperature in the Sb_2Te_3 column compared to Bi_2Te_3 column as noticed in Figs. 7 and 8. In the

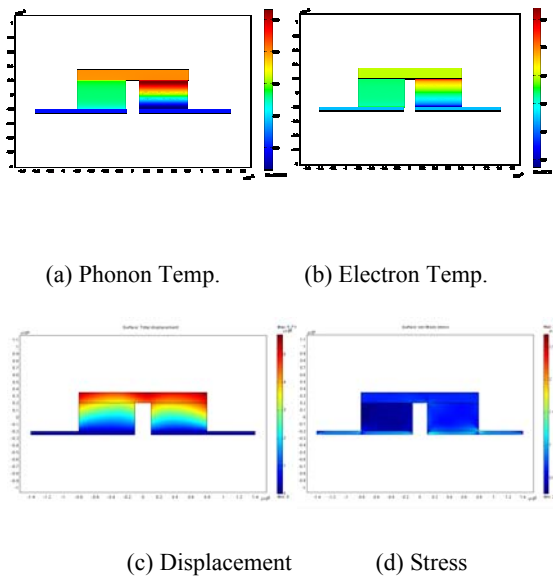


Fig. 6 2D Model result of Multiphysics analysis; (a) Phonon Temperature, (b) Electron Temperature, (c) Displacement, and (d) Stress distributions.

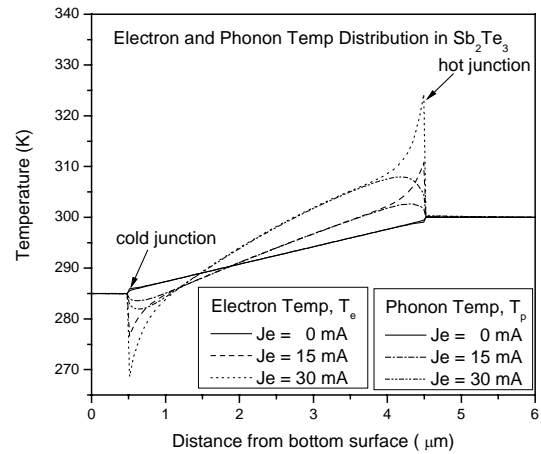


Fig. 7 Variations of electron and phonon temperatures along the height of Sb_2Te_3 (P type) thermoelectric column for different current inputs.

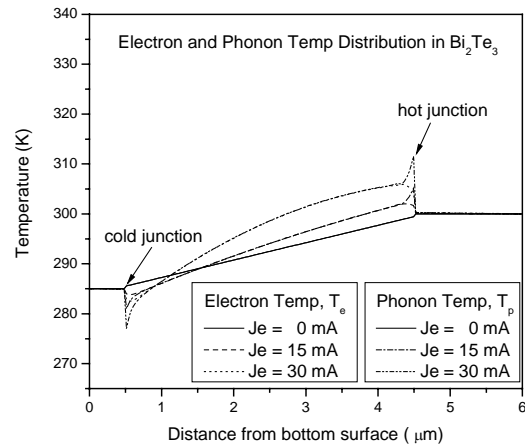


Fig. 8 Variations of electron and phonon temperatures along the height of Bi_2Te_3 (N type) thermoelectric column for different current inputs.

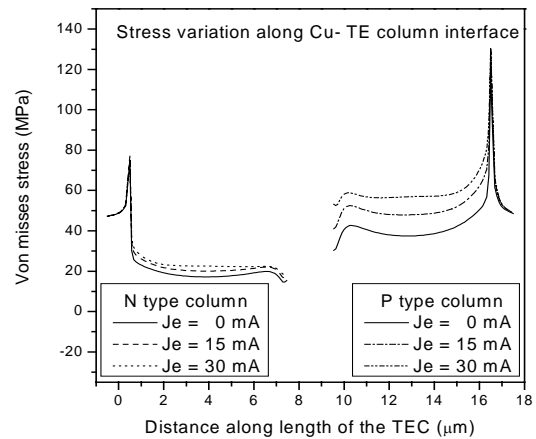


Fig. 9 Variations of stress at the interfaces between N and P type columns and the metal connectors.

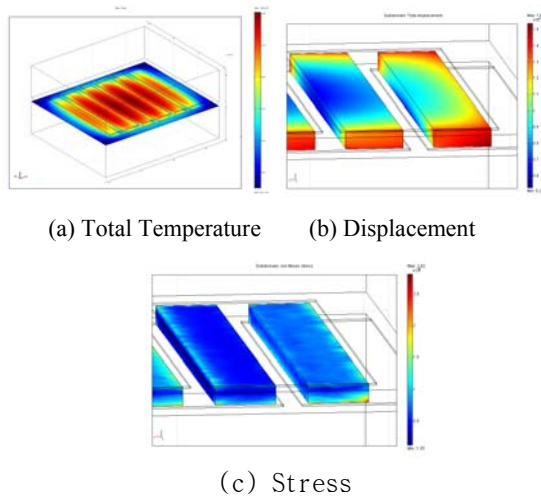


Fig. 10 3D Model result of Multiphysics analysis;
(a) Total Temperature, (b) Displacement, and (c)
Stress.

Table 4. Maximum stress developed in different parts
of the TEC at different current inputs.

Temperature (K)		285~300				
Current		4A	8A	12A	16A	20A
Max Stress [GPa]	Cu	1.66	1.71	1.78	1.87	1.99
	Sb ₂ Te ₃	1.38	1.42	1.47	1.55	1.64
	Bi ₂ Te ₃	0.78	0.80	0.83	0.88	0.93

model we used CTE values 13×10^{-6} , 16.5×10^{-6} and 20×10^{-6} for the Bi₂Te₃, Sb₂Te₃ and Cu respectively. It should be noted that the absolute values of thermal stress would depend upon the residual stress in the thermoelectric materials, which is determined by the fabrication temperature of the alloys. In our model we took the reference temperature to be 0 K. However while simulating real TECs, the reference temperature should be taken to be same as the fabrication temperature of the micro-TEC films.

Figs. 10 (a), (b) and (c) represent the total temperature, displacement and the stress distributions in the thermoelectric columns of the 3D model for $T_h = 285$ K, $T_c = 300$ K and $J_e = 8$ A.

The maximum stress developed in the Sb₂Te₃, Bi₂Te₃ and Cu films in case of $J_e = 0$ A were 1.375 GPa, 0.78 GPa and 1.64 GPa respectively. For $J_e = 15$ mA and 30 mA the stress values remained unchanged, indicating that the input current is too low to cause thermoelectric effect. The input current was then increased and the model was solved for 4, 8, 12, 16 and 20A. The maximum stresses developed in various components of the 3D model for $T_h = 300$ K, $T_c = 285$ K and $J_e = 4, 8, 12, 16$ and 20 A are summarized in Table 4. The table shows that at all current inputs, the maximum of the three stresses was that developed in the Cu- connector. At higher currents the stress increased in all parts of the TEC.

6. CONCLUSIONS

Thermoelectric thin films were prepared using co-sputtering method. Properties required for finite element analysis were obtained through nanoindentation test on the thin films and bulk materials, in conjunction with other means. An equation-based multiphysics model was developed for analyzing the insights of micro-thermoelectric coolers. Simulation with the developed model showed fascinating results. The developed model will be used for the design and development of micro-thermoelectric cooler in our ongoing research.

ACKNOWLEDGMENTS

This research was accomplished as a part of the project, "Technology Development of Advanced Cooling System" supported by Korea Research Council for Industrial Science and Technology. The authors gratefully appreciate the support.

NOMENCLATURE

k_p = Phonon thermal conductivity (W/mK)
 k_e = Electron thermal conductivity (W/mK)
 K_B = Boltzman constant 1.3006×10^{-23}
 T_p = Phonon Temperature
 T_e = Electron temperature
 n_c = Electron/hole concentration in the thermoelectric element (m^{-3})
 τ_e = Electron/hole energy relaxation time
 ρ_e = Electrical resistivity (Ωm)
 J_e = Current (A)
 A_{te} = Cross sectional area of thermoelectric column (m^2)
 R_c = Contact resistance (W/mK)
 δ = Electron-phonon cooling length (m)

REFERENCES

- [1] M.M. Alexandru and M. Mihaela, "A FEM analysis of thermoelectric and thermomagnetic phenomena in semiconductor materials" Vol. **, pp. ***, 1977.
- [2] D.R. Baselt, G.U. Lee, M. Natesan, S.W. Metzger, P.E. Sheeha and R.J. Colton, "A biosensor based on magnetoresistance technology" *Biosensors & Bioelectronics*, Vol. 13, pp. 731, 1998.
- [3] D.R. Baselt, G.U. Lee, K.M. Hansen, L.A. Chrisey and R.J. Colton, "A high sensitivity micromachined biosensor" *Proc. IEEE*, Vol. 85, No. 4, pp. 672, 1997.
- [4] L.D. Hicks and M.S. Dresselhaus, "Thermoelectric figure of merit of a one-dimensional conductor" *Phys. Rev.*, Vol. 47, No. B, pp. 12727, 1993.
- [5] R.Venkatasubramanian, E. Siivola, T.Colpitts and B. O'Quinn, "Thin-film thermoelectric devices with high room-temperature figures of merit", *Nature*, Vol. 413, pp.597-602, 2001.
- [6] H. Zou, D.M. Rowe and G. Min, "Growth of p- and n-type Bismuth telluride thin films by co-evaporation", *Journal of Crystalline Growth*, Vol. 222, pp. 82-87, 2001.
- [7] H. Zou, D.M. Rowe and S.G.K. Williams, "Peltier effect in a co-evaporated Sb₂Te₃(p)-Bi₂Te₃(n) thin film thermocouple", *Thin Solid Films*, Vol. 408, pp. 270-274,

- 2002.
- [8] G. Min and D.M. Rowe, "Cooling performance of integrated thermoelectric micro-cooler", *Solid-State Electron*, Vol. 43, pp. 923-929, 1999.
- [9] J.P. Fleurial, J.A. Herman, G.J. Snyder, M.A. Ryan, A. Borschevsky and C. Huang, "Electrochemical deposition of (Bi, Sb)₂Te₃ for thermoelectric micro-devices", *Mater. Res. Soc.*, Vol. 626, pp. Z11.3.1-Z11.3.8, 2000.
- [10] F. Völklein, V. Baier, U. Dillner and E. Kessler, "Transport properties of flash-evaporated (Bi_{1-x}Sb_x)₂Te₃ films I: Optimization of film properties", *Thin Solid Films*, Vol. 187, pp. 253-262, 1990.
- [11] A. Lopez-Otero, "Hot wall epitaxy", *Thin Solid Films*, Vol. 49, pp. 3-57, 1978.
- [12] A. Dauscher, A. Thomy and H. Scherrer, "Pulsed laser deposition of Bi₂Te₃ thin films", *Thin Solid Films*, Vol. 280, pp. 61-66, 2000.
- [13] A. Giani, F. Pascal-Delannoy, A. Boyer, A. Foucaran, M. Gschwind and P. Ancey, "Elaboration of Bi₂Te₃ by metal organic chemical vapor deposition", *Thin Solid Films*, Vol. 303, pp. 1-3, 1997.
- [14] A. Boyer and E. Cissé, "Properties of thin film thermoelectric materials: application to sensors using the Seebeck effect", *Material Science and Engineering-B*, Vol. 13, pp. 103-111, 1992.
- [15] Tai-Ran Hsu, MEMS and Microsystems design and manufacture, *McGraw Hill*, 2002.
- [16] L.W. da Silva and Massoud Kaviani, "Micro-thermoelectric cooler: interfacial effects on thermal and electrical transport", *International Journal of Heat and Mass Transfer*, Vol. 47, pp. 2417-2435, 2004.